A benchmark study on the thermal conductivity of nanofluids

Citation: Buongiorno, Jacopo et al. "A benchmark study on the thermal conductivity of nanofluids." Journal of Applied Physics 106 (2009): 094312. Copyright © 2009, American Institute of Physics

As Published: http://dx.doi.org/10.1063/1.3245330

Publisher: American Institute of Physics

Persistent URL: http://hdl.handle.net/1721.1/66196

Version: Final published version: final published article, as it appeared in a journal, conference proceedings, or other formally published context

A benchmark study on the thermal conductivity of nanofluids

Jacopo Buongiorno,[1,a)] David C. Venerus,[2] Naveen Prabhat,[1] Thomas McKrell,[1] Jessica Townsend,[3] Rebecca Christianson,[3] Yuriy V. Tolmachev,[4] Pawel Keblinski,[5] Lin-wen Hu,[1] Jorge L. Alvarado,[6] In Cheol Bang,[7,8] Sandra W. Bishnoi,[2] Marco Bonetti,[9] Frank Botz,[10] Anselmo Cecere,[11] Yun Chang,[12] Gang Chen,[1] Haisheng Chen,[13] Sung Jae Chung,[14] Minking K. Chyu,[14] Sarit K. Das,[15] Roberto Di Paola,[11] Yulong Ding,[13] Frank Dubois,[16] Grzegorz Dzido,[17] Jacob Eapen,[18] Werner Escher,[19,20] Denis Funfschilling,[21] Quentin Galand,[16] Jinwei Gao,[1] Patricia E. Gharagozloo,[22] Kenneth E. Goodson,[22] Jorge Gustavo Gutierrez,[23] Haiping Hong,[24] Mark Horton,[24] Kyo Sik Hwang,[25] Carlo S. Iorio,[16] Seok Pil Jang,[25] Andrzej B. Jarzebski,[17] Yiran Jiang,[2] Liwen Jin,[26] Stephan Kabelac,[27] Aravind Kamath,[6] Mark A. Kedzierski,[28] Lim Geok Kieng,[29] Chongyoup Kim,[30] Ji-Hyun Kim,[7] Seokwon Kim,[30] Seung Hyun Lee,[25] Kai Choong Leong,[26] Indranil Manna,[31] Bruno Michel,[19] Rui Ni,[21] Hrishikesh E. Patel,[15] John Philip,[32] Dimos Poulikakos,[20] Cecile Reynaud,[9] Raffaele Savino,[11] Pawan K. Singh,[15] Pengxiang Song,[33] Thirumalachari Sundararajan,[15] Elena Timofeeva,[34] Todd Tritcak,[10] Aleksandr N. Turanov,[4] Stefan Van Vaerenbergh,[16] Dongsheng Wen,[33] Sanjeeva Witharana,[13] Chun Yang,[26] Wei-Hsun Yeh,[2] Xiao-Zheng Zhao,[21] and Sheng-Qi Zhou[21]

[1]*Massachusetts Institute of Technology (MIT), 77 Massachusetts Avenue, Cambridge, Massachusetts 02139, USA*
[2]*Illinois Institute of Technology, 10 W. 33rd St., Chicago, Illinois 6016, USA*
[3]*Olin College of Engineering, Olin Way, Needham, Massachusetts 02492, USA*
[4]*Kent State University, Williams Hall, Kent, Ohio 44242, USA*
[5]*Materials Research Center, Rensselaer Polytechnic Institute (RPI), 110 8th Street, Troy, New York 12180, USA*
[6]*Texas A&M University, MS 3367, College Station, Texas 77843, USA*
[7]*School of Energy Engineering, Ulsan National Institute of Science and Technology, San 194 Banyeon-ri, Eonyang-eup, Ulju-gun, Ulsan Metropolitan City, Republic of Korea*
[8]*Tokyo Institute of Technology, 2-12-1 Ookayama, Meguro-ku, Tokyo 152-8550, Japan*
[9]*Commissariat à l'Énergie Atomique (CEA), IRAMIS, 91191 Gif sur Yvette, France*
[10]*METSS Corporation, 300 Westdale Avenue, Westerville, Ohio 43082, USA*
[11]*Department of Aerospace Engineering, University of Naples, P.le V. Tecchio 80, 80125 Naples, Italy*
[12]*SASOL of North America, 2201 Old Spanish Trail, Westlake, Louisiana 70669-0727, USA*
[13]*University of Leeds, Clarendon Road, Leeds LS2 9JT, United Kingdom*
[14]*Department of Mechanical Engineering and Materials Science, University of Pittsburgh, 648 Benedum Hall, 3700 O'Hara Street, Pittsburgh, Pennsylvania 15261, USA*
[15]*Department of Mechanical Engineering, Indian Institute of Technology-Madras, Chennai 600036, India*
[16]*Université Libre de Bruxelles, Chimie-Physique E.P. CP 165/62 Avenue P.Heger, Bat. UD3, Bruxelles 1050, Belgium*
[17]*Department of Chemical and Processing Engineering, Silesian University of Technology, ul. M. Strzody 7, 44-100 Gliwice, Poland*
[18]*Department of Nuclear Engineering, North Carolina State University, Raleigh, North Carolina 27695-7909, USA*
[19]*Zurich Research Laboratory, IBM Research GmbH, Saeumerstr. 4, CH-8803 Rüschlikon, Switzerland*
[20]*Department of Mechanical and Process Engineering, Laboratory of Thermodynamics in Emerging Technologies, ETH Zurich, 8092 Zurich, Switzerland*
[21]*Department of Physics, Chinese University of Hong Kong, G6, North Block, Science Center, Shatin NT, Hong Kong, China*
[22]*Stanford University, 440 Escondido Mall Rm 224, Stanford, California 94305, USA*
[23]*Department of Mechanical Engineering, University of Puerto Rico-Mayaguez, 259 Boulevard Alfonso Valdes, Mayaguez 00681, Puerto Rico*
[24]*South Dakota School of Mines and Technology, 501 E Saint Joseph Street, Rapid City, South Dakota 57701, USA*
[25]*School of Aerospace & Mechanical Engineering, Korea Aerospace University, 100, Hwajeon-dong, Deogyang-gu, Goyang-city, Gyeonggi-do 412-791, Republic of Korea*
[26]*School of Mechanical and Aerospace Engineering, Nanyang Technological University, 50 Nanyang Avenue, Singapore 639798, Singapore*
[27]*Institute for Thermodynamics, Helmut-Schmidt University Hamburg, D-22039 Hamburg, Germany*
[28]*National Institute of Standards and Technology (NIST), MS 863, Gaithersburg, Maryland 20899, USA*
[29]*DSO National Laboratories, 20 Science Park Drive, Singapore 118230, Singapore*
[30]*Korea University, Anam-dong, Sungbuk-ku, Seoul 136-713, Republic of Korea*
[31]*Department of Metallurgical and Materials Engineering, Indian Institute of Technology-Kharagpur, West Bengal 721302, India*

[a)]Author to whom correspondence should be addressed. Electronic mail: jacopo@mit.edu. Tel.: +1(617)253-7316.

[32]*SMARTS, NDED, Metallurgy and Materials Group, Indira Gandhi Centre for Atomic Research, Kalpakkam 603102, India*
[33]*School of Engineering and Materials Science, Queen Mary University of London, Mile End Road, London E1 4NS, United Kingdom*
[34]*Argonne National Laboratory, 9700 S. Cass Avenue, Argonne, Illinois 60439, USA*

(Received 12 June 2009; accepted 6 September 2009; published online 13 November 2009)

This article reports on the International Nanofluid Property Benchmark Exercise, or INPBE, in which the thermal conductivity of identical samples of colloidally stable dispersions of nanoparticles or "nanofluids," was measured by over 30 organizations worldwide, using a variety of experimental approaches, including the transient hot wire method, steady-state methods, and optical methods. The nanofluids tested in the exercise were comprised of aqueous and nonaqueous basefluids, metal and metal oxide particles, near-spherical and elongated particles, at low and high particle concentrations. The data analysis reveals that the data from most organizations lie within a relatively narrow band ($\pm 10\%$ or less) about the sample average with only few outliers. The thermal conductivity of the nanofluids was found to increase with particle concentration and aspect ratio, as expected from classical theory. There are (small) systematic differences in the absolute values of the nanofluid thermal conductivity among the various experimental approaches; however, such differences tend to disappear when the data are normalized to the measured thermal conductivity of the basefluid. The effective medium theory developed for dispersed particles by Maxwell in 1881 and recently generalized by Nan *et al.* [J. Appl. Phys. **81**, 6692 (1997)], was found to be in good agreement with the experimental data, suggesting that no anomalous enhancement of thermal conductivity was achieved in the nanofluids tested in this exercise. © *2009 American Institute of Physics*. [doi:10.1063/1.3245330]

I. INTRODUCTION

Engineered suspensions of nanoparticles in liquids, known recently as "nanofluids," have generated considerable interest for their potential to enhance the heat transfer rate in engineering systems, while reducing, or possibly eliminating, the issues of erosion, sedimentation and clogging that plagued earlier solid-liquid mixtures with larger particles. According to SciFinder Scholar, in 2008 alone 189 nanofluid-related publications (journal articles and patents) appeared (see Fig. 1), and it is estimated that more than 300 research groups and companies are engaged in nanofluids research worldwide. Furthermore, several review papers on nanofluid heat transfer have been published[1–7] and recently even a book entirely dedicated to nanofluids has been released.[8]

In spite of the attention received by this field, uncertainties concerning the fundamental effects of nanoparticles on thermophysical properties of solvent media remain. Thermal conductivity is the property that has catalyzed the attention of the nanofluids research community the most. As dispersions of solid particles in a continuous liquid matrix, nanofluids are expected to have a thermal conductivity that obeys the effective medium theory developed by Maxwell over 100 years ago.[9] Maxwell's model for spherical and well-dispersed particles culminates in a simple equation giving the ratio of the nanofluid thermal conductivity (k) to the thermal conductivity of the basefluid (k_f)

$$\frac{k}{k_f} = \frac{k_p + 2k_f + 2\phi(k_p - k_f)}{k_p + 2k_f - \phi(k_p - k_f)}, \tag{1}$$

where k_p is the particle thermal conductivity and ϕ is the particle volumetric fraction. Note that the model predicts no explicit dependence of the nanofluid thermal conductivity on the particle size or temperature. Also, in the limit of $k_p \gg k_f$ and $\phi \ll 1$, the dependence on particle loading is expected to be linear, as given by $k/k_f \approx 1+3\phi$. However, several deviations from the predictions of Maxwell's model have been reported, including:

- a strong thermal conductivity enhancement beyond that predicted by Eq. (1) with a nonlinear dependence on particle loading;[10–16]
- a dependence of the thermal conductivity enhancement on particle size and shape; and[15,17–25]
- a dependence of the thermal conductivity enhancement on fluid temperature.[20,26–28]

To explain these unexpected and intriguing findings, several hypotheses were recently formulated. For example, it was proposed that:

- particle Brownian motion agitates the fluid, thus creating a microconvection effect that increases energy transport;[29–33]

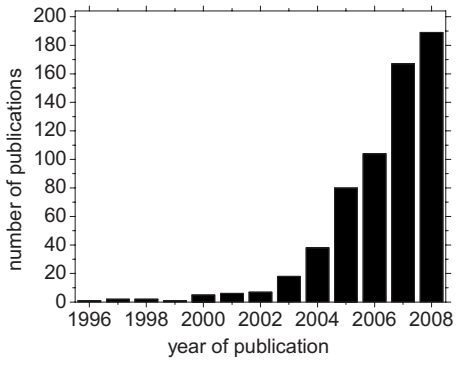

FIG. 1. Number of publications containing the term nanofluid according to SciFinder Scholar.

- clusters or agglomerates of particles form within the nanofluid, and heat percolates preferentially along such clusters;[34–39] and
- basefluid molecules form a highly ordered high-thermal-conductivity layer around the particles, thus augmenting the effective volumetric fraction of the particles.[34,38,40,41]

Experimental confirmation of these mechanisms has been weak; some mechanisms have been openly questioned. For example, the microconvection hypothesis has been shown to yield predictions in conflict with the experimental evidence.[25,42] In addition to theoretical inconsistencies, the nanofluid thermal conductivity data are sparse and inconsistent, possibly due to (i) the broad range of experimental approaches that have been implemented to measure nanofluid thermal conductivity (e.g., transient hot wire, steady-state heated plates, oscillating temperature, and thermal lensing), (ii) the often-incomplete characterization of the nanofluid samples used in those measurements, and (iii) the differences in the synthesis processes used to prepare those samples, even for nominally similar nanofluids. In summary, the possibility of very large thermal conductivity enhancement in nanofluids beyond Maxwell's prediction and the associated physical mechanisms are still a hotly debated topic.

At the first scientific conference centered on nanofluids (*Nanofluids: Fundamentals and Applications*, September 16–20, 2007, Copper Mountain, Colorado), it was decided to launch an international nanofluid property benchmark exercise (INPBE), to resolve the inconsistencies in the database and help advance the debate on nanofluid properties. This article reports on the INPBE effort, and in particular on the thermal conductivity data. Other property data collected in INPBE (prominently viscosity) will be reported in a separate publication in the near future. The article is structured as follows. The INPBE methodology is described in Sec. II. The nanofluid samples used in the exercise are described in Sec. III. The thermal conductivity data are presented in Sec. IV. The thermal conductivity data are compared with the effective medium theory predictions in Sec. V. The findings are summarized in Sec. VI.

II. INPBE METHODOLOGY

The exercise's main objective was to compare thermal conductivity data obtained by different organizations for the same samples. Four sets of test nanofluids were procured (see Sec. III). To minimize spurious effects due to nanofluid preparation and handling, all participating organizations were given identical samples from these sets and were asked to adhere to the same sample handling protocol. The exercise was "semiblind," as only minimal information about the samples was given to the participants at the time of sample shipment. The minimum requirement to participate in the exercise was to measure and report the thermal conductivity of at least one test nanofluid at room temperature. However, participants could also measure (at their discretion) thermal conductivity at higher temperature and/or various other nanofluid properties, including (but not necessarily limited to) viscosity, density, specific heat, particle size and concentration. The data were then reported in a standardized form to the exercise coordinator at the Massachusetts Institute of Technology (MIT) and posted, unedited, at the INPBE website (http://mit.edu/nse/nanofluids/benchmark/index.html). The complete list of organizations that participated in INPBE, along with the data they contributed, is reported in Table I. INPBE climaxed in a workshop, held on January 29–30 2009 in Beverly Hills, California, where the results were presented and discussed by the participants. The workshop presentations can also be found at the INPBE website.

III. TEST NANOFLUIDS

To strengthen the generality of the INPBE results, it was desirable to select test nanofluids with a broad diversity of parameters; for example, we wanted to explore aqueous and nonaqueous basefluids, metallic and oxidic particles, near-spherical and elongated particles, and high and low particle loadings. Also, given the large number of participating organizations, the test nanofluids had to be available in large quantities (>2 l) and at reasonably low cost.

Accordingly, four sets of test samples were procured. The providers were Sasol (set 1), DSO National Laboratories (set 2), W. R. Grace & Co. (set 3), and the University of Puerto Rico at Mayaguez (set 4). The providers reported information regarding the particle materials, particle size and concentration, basefluid material, the additives/stabilizers used in the synthesis of the nanofluid, and the material safety data sheets. Said information was independently verified, to the extent possible, by the INPBE coordinators (MIT and Illinois Institute of Technology, IIT), as reported in the next sections. Identical samples were shipped to all participating organizations.

A. Set 1

The samples in set 1 were supplied by Sasol. The numbering for these samples is as follows:

(1) alumina nanorods in de-ionized water,
(2) de-ionized water (basefluid sample),
(3) alumina nanoparticles (first concentration) in polyalphaolefins lubricant (PAO)+surfactant,
(4) alumina nanoparticles (second concentration) in PAO+surfactant,
(5) alumina nanorods (first concentration) in PAO+surfactant
(6) alumina nanorods (second concentration) in PAO+surfactant, and
(7) PAO+surfactant (basefluid sample).

The synthesis methods have not been published, so a brief summary is given here. For sample 1, alumina nanorods were simply added to water and dispersed by sonication. Sample 2, de-ionized water, was not actually sent to the participants. The synthesis of samples 3–7 involved three steps. First, the basefluid was created by mixing PAO (SpectraSyn-10 by Exxon Oil) and 5 wt % dispersant (Solsperse 21000 by Lubrizol Chemical), and heating and stirring the mixture at 70 °C for 2 h, to ensure complete dissolution of the dispersant. Second, hydrophilic alumina nanoparticles

TABLE I. Participating organizations in and data generated for INPBE.

Organization/contact person	Experimental method[a] for thermal conductivity measurement (Ref.)	Generated data for			
		Set 1	Set 2	Set 3	Set 4
Argonne National Laboratory/E. V. Timofeeva	KD2 Pro	TC[b]	TC	TC	TC
CEA/C. Reynaud	Steady-state coaxial cylinders[c]	TC			
Chinese University of Hong Kong/S.-Q. Zhou	Steady state parallel plate[d]	*V* [e]	TC, *V*	TC, *V*	
DSO National Laboratories/L. G. Kieng	Supplied nanofluid samples				
ETH Zurich and IBM Research/W. Escher	THW and parallel hot plates[f]	TC	TC	TC	TC
Helmut-Schmidt University Armed Forces/ S. Kabelac	Guarded hot plate[d]		TC, *V*	TC, *V*	TC, *V*
Illinois Institute of Technology/D. Venerus	Forced Rayleigh scattering[g]	TC, *V*	TC		
Indian Institute of Technology, Kharagpur/ I. Manna	KD2 Pro	TC	TC	TC	TC
Indian Institute of Technology, Madras/T. Sundararajan, S. K. Das	THW[h]	TC	TC		
Indira Gandhi Centre for Atomic Research/J. Philip	THW[d], KD2	TC	TC	TC	
Kent State University/Y. Tolmachev	KD2 Pro	TC	TC, *V*	TC	TC
Korea Aerospace University/S. P. Jang	THW[i]			TC	
Korea Univ./C. Kim	THW[d]	TC, *V*	TC, *V*	TC, *V*	
METSS Corp./F. Botz	THW[d]	TC	TC	TC	
MIT/J. Buongiorno, L.W. Hu, T. McKrell	THW[j]	TC	TC	TC	TC
MIT/G. Chen	THW[k]		TC	TC, *V*	
Nanyang Technological University/K. C. Leong	THW[l]	TC			TC
NIST/M. A Kedzierski	KD2 Pro	TC, *V*, *D* [m]	*V*, *D*	*V*, *D*	*V*, *D*
North Carolina State University-Raleigh/J. Eapen	Contributed to data analysis				
Olin College of Engineering/R. Christianson, J. Townsend	THW[n]	TC, *V*	TC		
Queen Mary University of London/D. Wen	THW[d]	TC, *V*	TC	TC	TC
RPI/P. Keblinski	Contributed to data analysis				
SASOL of North America/Y. Chang	Supplied nanofluid samples				
Silesian University of Technology/A. B. Jarzebski, G. Dzido	THW[o]			TC, *V*	TC, *V*
South Dakota School of Mines and Technology/H. Hong	Hot Disk[p]	TC	TC	TC	TC
Stanford University/P. Gharagozloo, K. Goodson	IR thermometry[q]	TC	TC	TC	
Texas A&M University/J. L. Alvarado	KD2 Pro	TC	TC	TC	TC
Ulsan National Institute of Science and Technology; Tokyo Institute of Technology/I. C. Bang, J. H. Kim	KD2 Pro	TC, *V*	TC, *V*	TC, *V*	TC, *V*
Université Libre de Bruxelles, University of Naples/C. S. Iorio	Modified hot wall technique[r], Parallel plates[s]		TC, *V*, *D*	TC, *V*, *D*	
University of Leeds/Y. Ding	KD2 and parallel hot plates[t]	TC, *V*	TC	TC, *V*	TC, *V*
University of Pittsburgh/M. K. Chyu	Unitherm™ 2022 (Guarded heat flow meter)	TC	TC	TC, *V*	
University of Puerto Rico-Mayaguez/J. G. Gutierrez	THW[u]			TC	TC

[a]THW=transient hot wire; KD2 and KD2 Pro (information about these devices at http://www.decagon.com/thermal/instrumentation/instruments.php); Unitherm™ 2022 (information about this device at http://anter.com/2022.htm).
[b]TC=thermal conductivity.
[c]Reference 61.
[d]A publication with detailed information about this apparatus is not available.
[e]*V*=viscosity.
[f]Reference 62.
[g]Reference 63.
[h]Reference 33.
[i]Reference 64.
[j]Reference 65.
[k]Reference 66.
[l]Reference 19.
[m]*D*=density.
[n]Reference 67.
[o]Reference 68.
[p]Reference 69.
[q]Reference 70.
[r]Reference 71.
[s]Reference 28.
[t]Reference 72.
[u]Reference 73.

TABLE II. Characteristics of the set 1 samples.

	Loading		Particle size		
Sample	Sasol	MIT [a]	Sasol	MIT	IIT[b]
1	1 vol %	1.2–1.3 vol %[c]	80 nm×10 nm (nominal nanorod size),	60–64 nm[d]	131–134 nm
2	n/a[e]	n/a	n/a	n/a	n/a
3	1 vol %	0.7–0.8 vol %[f]	10 nm (nominal particle size)	[g]	75–88 nm
4	3 vol %	1.9–2.2 vol %[f]	10 nm (nominal particle size)	[g]	99–112 nm
5	1 vol %	0.7–0.8 vol %[f]	80×10 nm^2 (nominal nanorod size)	[g]	70–110 nm
6	3 vol %	2.0–2.3 vol %[f]	80×10 nm^2 (nominal nanorod size)	[g]	100–115 nm
7	n/a	n/a	n/a	n/a	n/a

[a]Range of values is given to account for expected hydration range of alumina (boehmite). Boehmite's chemical formula is $Al_2O_3 \cdot nH_2O$, where $n=1$ to 2. The hydrate is bound and cannot be dissolved in water. In most boehmites there is 70–82 wt % Al_2O_3 per gram of powder. Boehmite density is 3.04 g/cm^3.
[b]Average size of dispersed phase, measured by dynamic light scattering (DLS). The range indicates the spread of six nominally identical measurements. DLS systemic uncertainty is of the order of ±10 nm. Malvern NanoS used to collect data.
[c]Measurements by inductive coupled plasma (ICP).
[d]Average size of dispersed phase, measured by DLS. The range indicates the spread of multiple nominally identical measurements. DLS systemic uncertainty is of the order of ±10 nm.
[e]Not applicable.
[f]Measurements by neutron activation analysis (NAA).
[g]Not available due to unreliability of DLS analyzer with PAO-based samples.

or nanorods (in aqueous dispersion) were coated with a monolayer of hydrophobic linear alkyl benzene sulfonic acid and then spray dried. Third, the dry nanoparticles or nanorods were dispersed into the basefluid.

Table II reports the information received by Sasol along with the results of some measurements done at MIT and IIT. Figure 2 shows transmission electron microscopy (TEM) images for samples 1 and 3. TEM images for samples 4–6 are not available.

B. Set 2

The samples in set 2 were supplied by Dr. Lim Geok Kieng of DSO National Laboratories in Singapore. The numbering for these samples is as follows:

(1) gold nanoparticles in de-ionized water and trisodium citrate stabilizer and

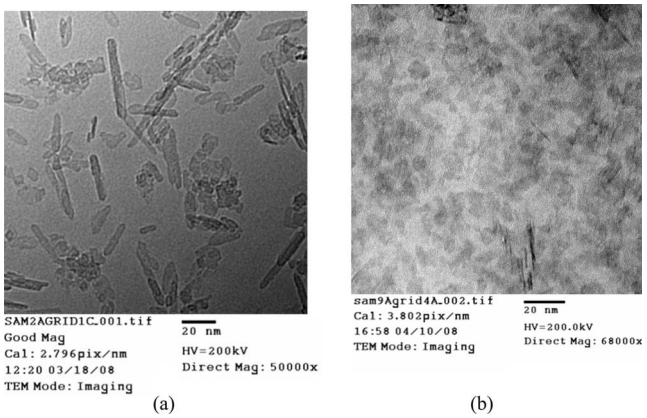

FIG. 2. Set 1—TEM pictures of samples 1 (a) and 3 (b), respectively. The nanorod dimensions in sample 1 are in reasonable agreement with the nominal size (80 nm×10 nm) stated by Sasol. However, smaller particles of lower aspect ratio are clearly present along with the nanorods. TEM pictures of PAO-based samples have generally been of lower quality. However, the nanoparticles in sample 3 appear to be roughly spherical and of approximate diameter 10–20 nm, thus consistent with the nominal size of 10 nm stated by Sasol.

(2) de-ionized water+sodium citrate stabilizer (basefluid sample).

The nanofluid sample was produced according to a one-step "citrate method," in which 100 ml of 1.18 m*M* gold(III) chloride trihydrate solution and 10 ml of 3.9 m*M* trisodium citrate dehydrate solution were mixed, brought to boil and stirred for 15 min. Gold nanoparticles formed as the solution was let cool to room temperature. Table III reports the information received by DSO National Laboratories along with the results of some measurements done at MIT and IIT. Figure 3 shows the TEM images for sample 1.

C. Set 3

Set 3 consisted of a single sample, supplied by W. R. Grace & Co.Silica monodispersed spherical nanoparticles and stabilizer in de-ionized water. The silica particles were synthesized by ion exchange of sodium silicate solution in a proprietary process. A general description of this process can be found in the literature.[43] Grace commercializes this nanofluid as Ludox TM-50, and indicated that the nanoparticles are stabilized by making the system alkaline, the base being deprotonated silanol (SiO^-) groups on the surface with Na^+ as the counterion (0.1–0.2 wt % of Na ions). The dispersion contains also 500 ppm of a proprietary biocide. Grace stated that it was not possible to supply a basefluid sample with only water and stabilizer "because of the way the particles are made." Given the low concentration of the stabilizer and biocide, de-ionized water was assumed to be the basefluid sample, and designated "sample 2," though it was not actually sent to the participants. Table IV reports the information received by Grace along with the results of some measurements done at MIT. Figure 4 shows the TEM images for the set 3 sample.

D. Set 4

The samples in set 4 were supplied by Dr. Jorge Gustavo Gutierrez of the University of Puerto Rico-Mayaguez

TABLE III. Characteristicsf the set 2 samples.

	Au loading		Particle size			Stabilizer concentration (trisodium citrate)		*p*H
Sample	DSO	MIT[a]	DSO	MIT[b]	IIT[c]	DSO (wt %)	MIT[a] (wt %)	MIT
1	0.0010 vol %	0.0009 vol %[d]	20–30 nm	4–11 nm	14.8 nm ave (10–22 nm)	0.1	0.10	6.01
2	0	0[e]	n/a[f]	n/a	n/a	0.1	0.09	7.30

[a]Measurements by inductive coupled plasma (ICP). ICP has an accuracy of 0.6% of the reported value for gold in the concentration range of interest.
[b]Number-weighted average size of particles, measured by DLS. The range indicates the spread of two nominally identical measurements. DLS systemic uncertainty is of the order of ±10 nm.
[c]Measurements by DLS. The values reported are the number-weighted average and the range at the full-width half maximum for six measurements.
[d]Assumed density of gold is 19.32 g/cm^3.
[e]Within the detection limit of ICP.
[f]Not applicable.

(UPRM). A chemical coprecipitation method was used to synthesize the particles.[44] The set 4 sample numbering is as follows:

(1) Mn–Zn ferrite ($Mn_{1/2}$–$Zn_{1/2}$–Fe_2O_4) particles in solution of stabilizer and water and
(2) solution of stabilizer (25 wt %) and water (75 wt %) (basefluid sample).

The stabilizer is tetramethylammonium hydroxide or $(CH_3)_4NOH$. Table V reports the information received by UPRM along with the results of some measurements done at MIT. Figure 5 shows the TEM images for sample 1.

IV. THERMAL CONDUCTIVITY DATA

The thermal conductivity data generated by the participating organizations are shown in Figs. 6–18, one for each sample in each set. In these figures the data are anonymous, i.e., there is no correspondence between the organization number in the figures and the organization list in Table I. The data points indicate the mean value for each organization, while the error bars indicate the standard deviation calculated using the procedure described in Appendix A. The sample average, i.e., the average of all data points, is shown as a solid line, and the standard error of the mean is denoted by the dotted lines to facilitate visualization of the data spread. The standard error of the mean is typically much lower than the standard deviation because it takes into account the total number of measurements made to arrive at the sample average. Each measurement technique is denoted by a different symbol, and averages for each of the measurement techniques are shown. The measurement techniques were grouped into four categories: the KD2 thermal properties analyzer (Decagon), custom thermal hot wire (THW), steady state parallel plate, and other techniques. Outliers (determined using Peirce's criterion) are shown as filled data points and were not included in either the technique or ensemble averages.

It can be seen that for all water-based samples in all four sets most organizations report values of the thermal conductivity that are within ±5% of the sample average. For the PAO-based samples the spread is a little wider with most organizations reporting values that are within ±10% of the sample average. A note of caution is in order: while all data reported here are nominally for room temperature, what constitutes "room temperature" varies from organization to organization. The data shown in Figs. 6–18 include only measurements conducted in the range of 20–30 °C. Over this range of temperatures, the thermal conductivity of the test fluids is expected to vary minimally; for example, the water thermal conductivity varies by less than 2.5%. Where deionized water was the basefluid (Figs. 7 and 16), the range of nominal thermal conductivity of water for 20–30 °C is shown as a red band plotted on top of the measured data.

Figures 19–26 show the thermal conductivity "enhance-

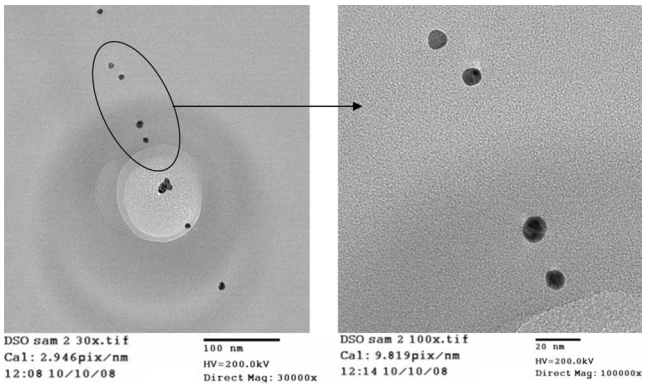

FIG. 3. Set 2—TEM pictures of sample 1. The nanoparticles are roughly spherical and of diameter <20 nm, thus somewhat smaller than the nominal size of 20–30 nm stated by DSO National Laboratories.

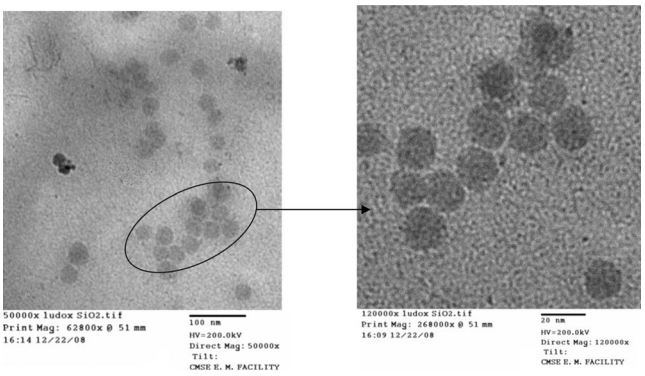

FIG. 4. Set 3—TEM pictures of sample 1. The nanoparticles are roughly spherical and of diameter 20–30 nm, thus consistent with the nominal size of 22 nm stated by Grace.

TABLE IV. Characteristics of the set 3 samples.

	Silica (SiO_2) loading		Na_2SO_4 concentration		Particle size		*p*H	
Sample	Grace	MIT	Grace	MIT[a]	Grace	MIT[b]	Grace	MIT
1	49.8 wt % 31.1 vol %[c]	43.6 wt % [a] 26.0 vol %[c]	0.1–0.2 wt % of Na	0.27 wt % of Na	22 nm	20–40 nm	8.9	9.03
2[d]	n/a[e]	n/a	n/a	n/a	n/a	n/a	n/a	n/a

[a]Measured by inductive coupled plasma (ICP). ICP has an accuracy of 0.6% of the reported value.
[b]Number-weighted average size of particles, measured by dynamic light scattering (DLS). The range indicates the spread of three nominally identical measurements. DLS systemic uncertainty is of the order of ± 10 nm.
[c]Assumed density of silica (SiO_2) is 2.2 g/cm^3.
[d]Sample 2 is simply de-ionized water, which was assumed to be the basefluid sample, but was not actually sent to the participants.
[e]Not applicable.

TABLE V. Characteristics of the set 4 samples.

	Particle loading		Particle composition		Particle size		*p*H
Sample	UPRM	MIT	UPRM	MIT[a]	UPRM	MIT	MIT
1	0.17 vol %[b]	0.16 vol %[c]	$Mn_{1/2}$–$Zn_{1/2}$–Fe_2 [d]	Mn ~ 15 at. %, Zn ~ 14 at. %, Fe ~ 71 at. %	7.4 nm[e]	6–11 nm[f]	15.2
2	n/a[g]	n/a	n/a	n/a	n/a	n/a	15.1

[a]Atomic fraction of metals measured by energy dispersive x-ray spectroscopy (EDS).
[b]Determined from magnetic measurements.
[c]Measurements by inductive coupled plasma (ICP). Assumed density of 4.8 g/cm^3 for Mn–Zn ferrite. ICP has an accuracy of 0.6% of the reported value.
[d]The molar fraction of Mn and Zn was determined from stoichiometric balance.
[e]Average magnetic particle diameter.
[f]Number-weighted average size of particles, measured by dynamic light scattering (DLS). The range indicates the spread of four nominally identical measurements. DLS systemic uncertainty is of the order of ± 10 nm.
[g]Not applicable.

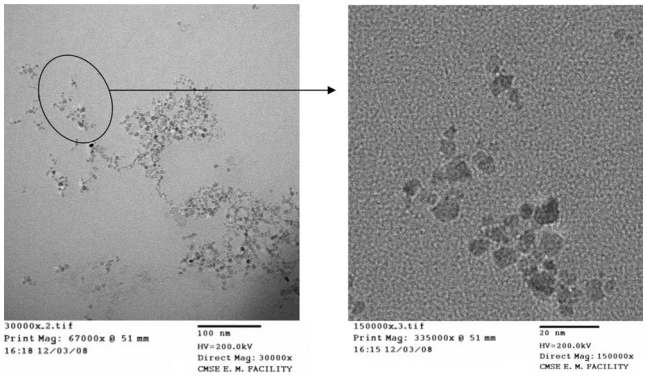

FIG. 5. Set 4—TEM pictures of sample 1. The nanoparticles have irregular shape and approximate size <20 nm, thus consistent with the nominal size of ~ 7 nm stated by UPRM.

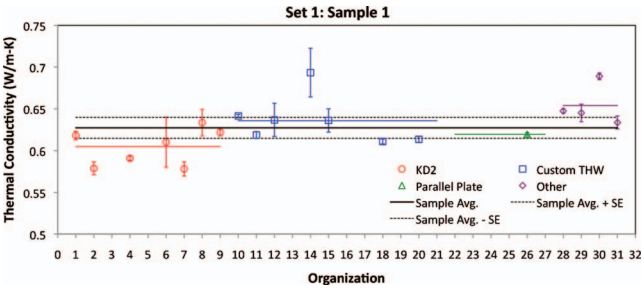

FIG. 6. (Color) Thermal conductivity data for sample 1, set 1.

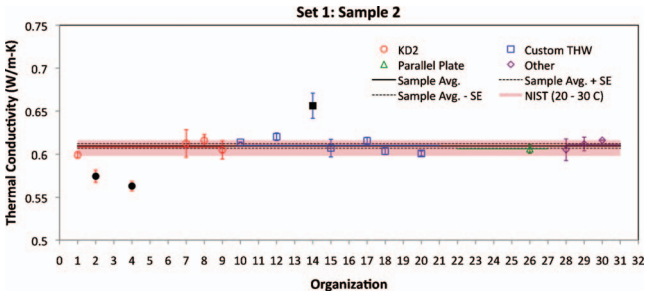

FIG. 7. (Color) Thermal conductivity data for sample 2 (basefluid), set 1.

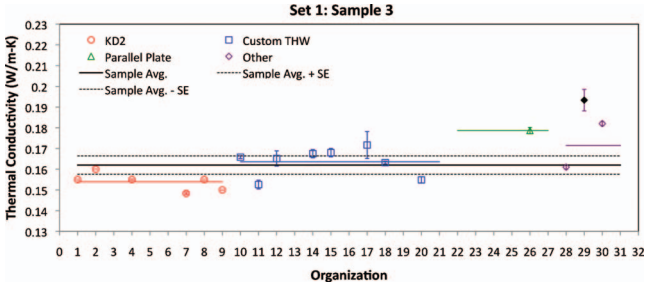

FIG. 8. (Color) Thermal conductivity data for sample 3, set 1.

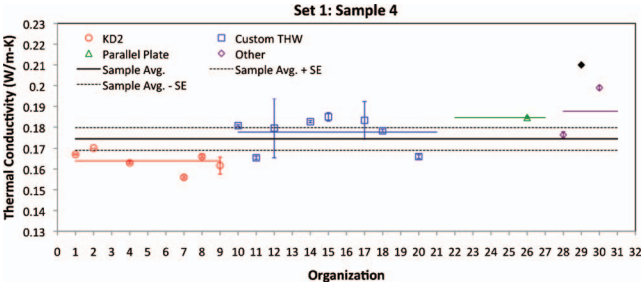

FIG. 9. (Color) Thermal conductivity data for sample 4, set 1.

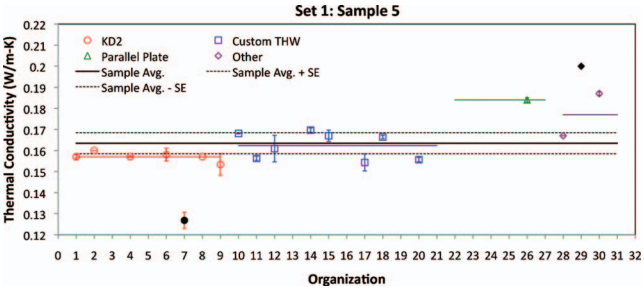

FIG. 10. (Color) Thermal conductivity data for sample 5, set 1.

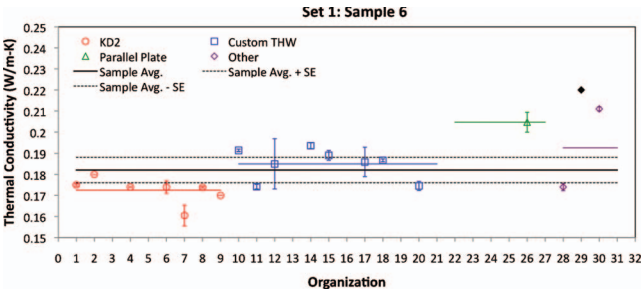

FIG. 11. (Color) Thermal conductivity data for sample 6, set 1.

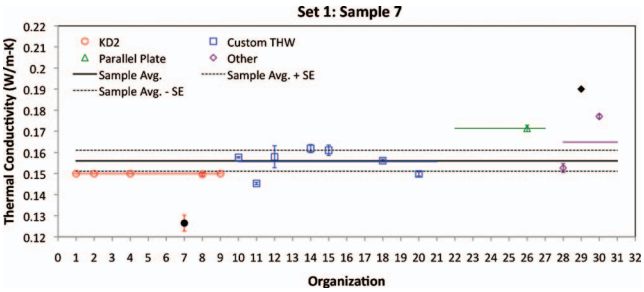

FIG. 12. (Color) Thermal conductivity data for sample 7, set 1.

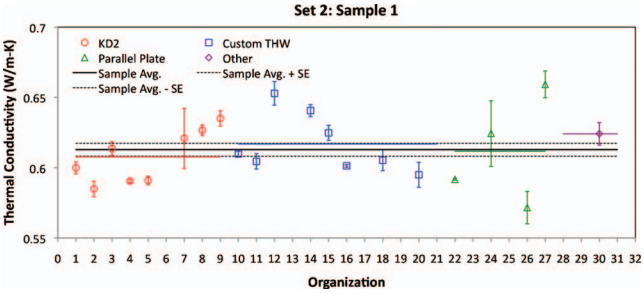

FIG. 13. (Color) Thermal conductivity data for sample 1, set 2.

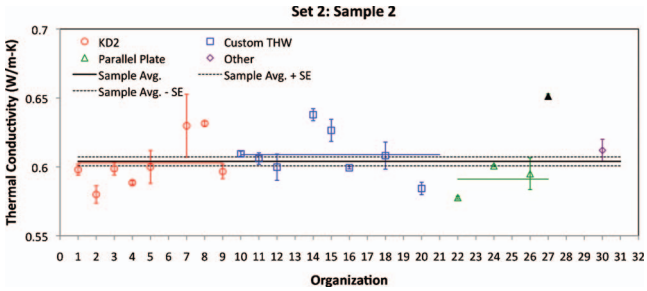

FIG. 14. (Color) Thermal conductivity data for sample 2, set 2.

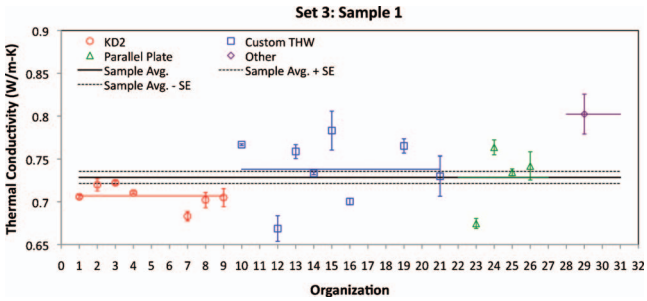

FIG. 15. (Color) Thermal conductivity data for sample 1, set 3.

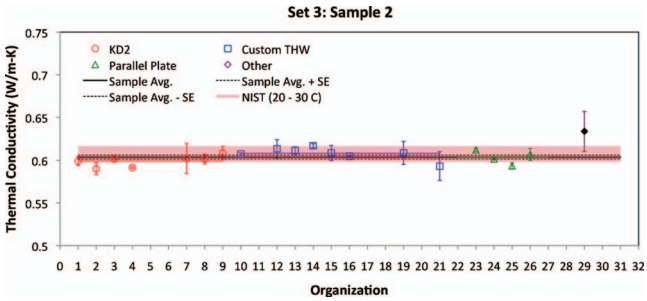

FIG. 16. (Color) Thermal conductivity data for sample 2 (basefluid), set 3.

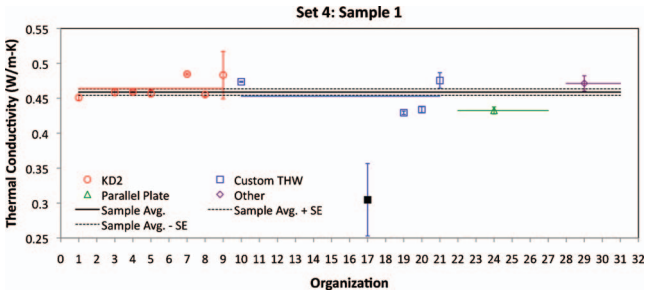

FIG. 17. (Color) Thermal conductivity data for sample 1, set 4.

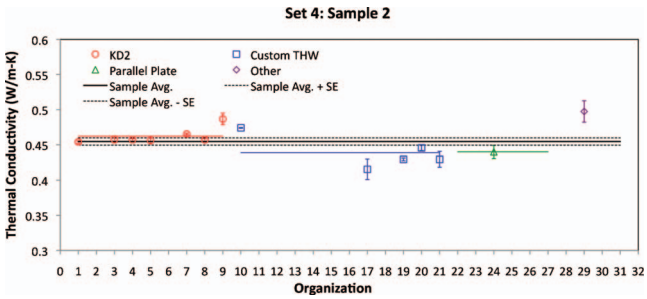

FIG. 18. (Color) Thermal conductivity data for sample 2 (basefluid), set 4.

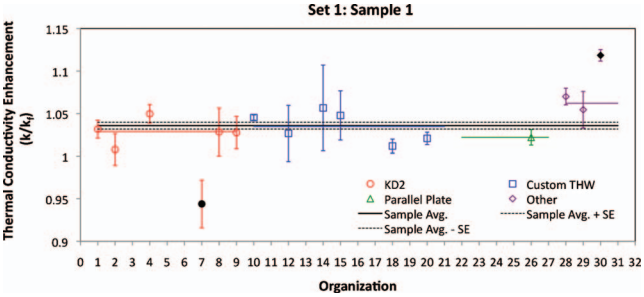

FIG. 19. (Color) Thermal conductivity enhancement data for sample 1, set 1.

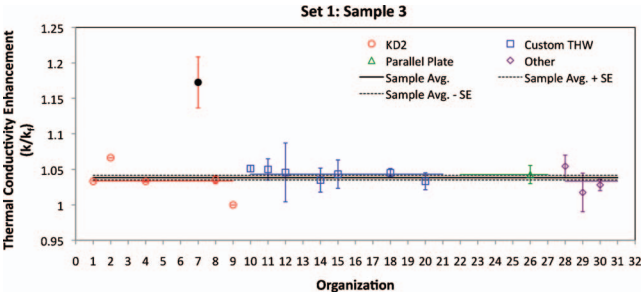

FIG. 20. (Color) Thermal conductivity enhancement data for sample 3, set 1.

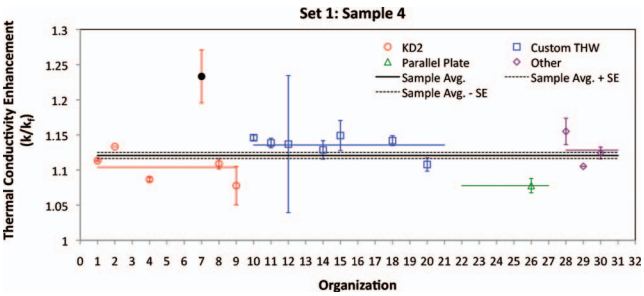

FIG. 21. (Color) Thermal conductivity enhancement data for sample 4, set 1.

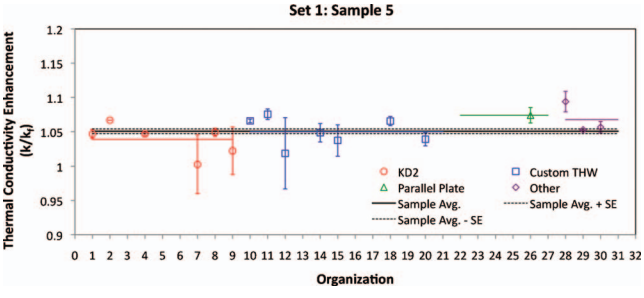

FIG. 22. (Color) Thermal conductivity enhancement data for sample 5, set 1.

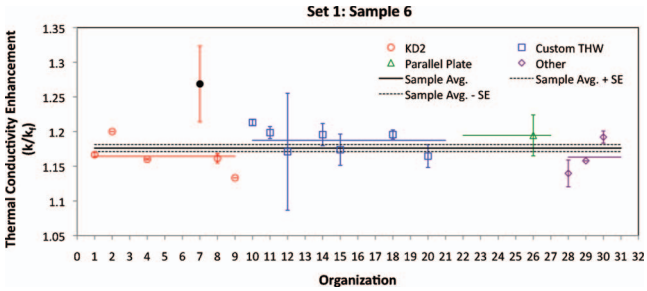

FIG. 23. (Color) Thermal conductivity enhancement data for sample 6, set 1.

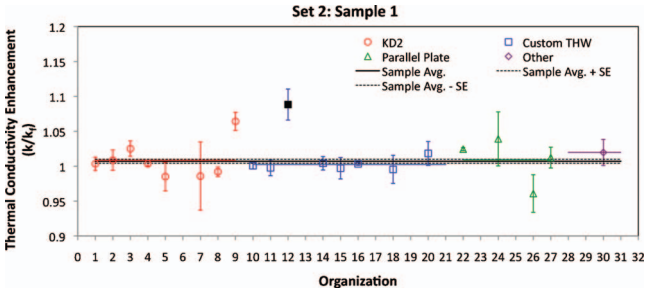

FIG. 24. (Color) Thermal conductivity enhancement data for sample 1, set 2.

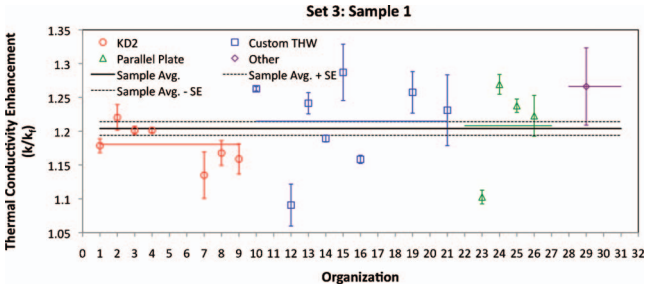

FIG. 25. (Color) Thermal conductivity enhancement data for sample 1, set 3.

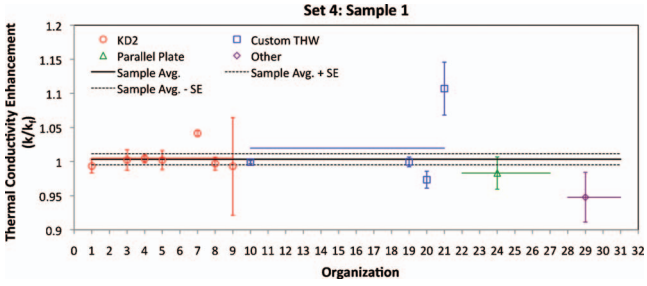

FIG. 26. (Color) Thermal conductivity enhancement data for sample 1, set 4.

TABLE VI. Summary of INPBE results.

Sample		Sample description[a]	Measured thermal conductivity[b] (W/m K)	Measured thermal conductivity ratio[b] k/k_f	Predicted thermal conductivity ratio[c] k/k_f	
					Lower bound	Upper bound
Set 1	Sample 1	Alumina nanorods (80×10 nm^2), 1 vol % in water	0.627 ± 0.013	1.036 ± 0.004	1.024	1.086
	Sample 2	De-ionized water	0.609 ± 0.003	n/a[d]	n/a	n/a
	Sample 3	Alumina nanoparticles (10 nm), 1 vol % in PAO+surfactant	0.162 ± 0.004	1.039 ± 0.003	1.027	1.030
	Sample 4	Alumina nanoparticles (10 nm), 3 vol % in PAO+surfactant	0.174 ± 0.005	1.121 ± 0.004	1.083	1.092
	Sample 5	Alumina nanorods (80×10 nm^2), 1 vol % in PAO+surfactant	0.164 ± 0.005	1.051 ± 0.003	1.070	1.116
	Sample 6	Alumina nanorods (80×10 nm^2), 3 vol % in PAO+surfactant	0.182 ± 0.006	1.176 ± 0.005	1.211	1.354
	Sample 7	PAO+surfactant	0.156 ± 0.005	n/a	n/a	n/a
Set 2	Sample 1	Gold nanoparticles (10 nm), 0.001 vol % in Water+stabilizer	0.613 ± 0.005	1.007 ± 0.003	1.000	1.000
	Sample 2	Water+stabilizer	0.604 ± 0.003	n/a	n/a	n/a
Set 3	Sample 1	Silica nanoparticles (22 nm), 31 vol % in Water+stabilizer	0.729 ± 0.007	1.204 ± 0.010	1.008	1.312
	Sample 2	De-ionized water	0.604 ± 0.002	n/a	n/a	n/a
Set 4	Sample 1	Mn–Zn ferrite nanoparticles (7 nm), 0.17 vol % in Water +stabilizer	0.459 ± 0.005	1.003 ± 0.008	1.000	1.004
	Sample 2	Water+stabilizer	0.455 ± 0.005	n/a	n/a	n/a

[a]Nominal values for nanoparticle concentration and size.
[b]Sample average and standard error of the mean.
[c]Calculated with the assumptions in Appendix B.
[d]Not applicable.

ment" for all nanofluid samples, i.e., the ratio of the nanofluid thermal conductivity to the basefluid thermal conductivity. For each organization, the data point represents the ratio of the mean thermal conductivities of the nanofluid and basefluid, while the error bars represent the standard deviation calculated according to the procedure described in Appendix A. If a participating organization did not measure the basefluid thermal conductivity in their laboratory, a calculation of enhancement was not made. Again, the sample average is shown as a solid line along with the standard error of the mean, and outliers are indicated by filled data points. Note that there is reasonable consistency (within $\pm5\%$) in the thermal conductivity ratio data among most organizations and for all four sets, including water-based and PAO-based samples.

The INPBE database is summarized in Table VI. Comparing the data for samples 3, 4, 5, and 6 in set 1, it is noted that, everything else being the same, the thermal conductivity enhancement is higher at higher particle concentration, and higher for elongated particles than for near-spherical particles. Comparing the data for samples 1 and 5 in set 1, it is noted that the thermal conductivity enhancement is somewhat higher for the PAO basefluid than for water. The set 2 data suggest that the thermal conductivity enhancement is negligible, if the particle concentration is very low, even if metal particles of high thermal conductivity are used. On the other hand, the set 3 data suggest that a robust enhancement can be achieved, if the particle concentration is high, even if the particle material has a modest thermal conductivity. All these trends are expected, based on the effective medium theory, as will be discussed in Sec. V below.

A. Effects of the experimental approach on the thermal conductivity measurements

Table I reports the experimental techniques used by the various organizations to measure thermal conductivity, and provides, when available, a reference where more information about those techniques can be found. Transient, steady-state, and optical techniques were used to measure thermal conductivity. There are transient measurement techniques that require the immersion of a dual heating and sensing element in the sample, such as the transient hot wire (THW) and transient hot disk techniques. The THW technique is based on the relationship between the thermal response of a very small (<100 μm) diameter wire immersed in a fluid sample to a step change in heating and the thermal conductivity of the fluid sample.[45] The THW technique was used by over half of the participating organizations, many of which used a custom built apparatus. The KD2 thermal properties analyzer made by Decagon, an off-the-shelf device that is based on the THW approach, was also used. The transient hot disk technique is similar to the THW technique, except that the heater/sensor is a planar disk coated in Kapton.[46] In steady-state techniques such as the parallel plate[47] and coaxial cylinder[48] methods, heat is transferred between two plates (or coaxial cylinders) sandwiching the test fluid. Measurement of the temperature difference and heat transfer rate across the fluid can be used to determine the thermal conductivity via Fourier's law. The thermal comparator method, also a steady-state method, measures the voltage difference between a heated probe in point contact with the surface of the fluid sample and a reference, which can be converted to thermal conductivity using a calibration curve of samples of known conductivity.[49] In the forced Rayleigh scattering method, an optical grating is created in a sample of the fluid using the intersection of two beams from a high-powered laser. The resulting temperature change causes small-scale density changes that create a refraction index grating that can be detected using another laser. The relaxation time of the refraction index grating is related to the thermal diffusivity of the fluid from which the thermal conductivity can be evaluated.[50]

The measurement techniques were grouped into KD2, custom THW, parallel plate, and other (which include thermal comparator, hot disk, forced Rayleigh scattering, and coaxial cylinders). Thermal conductivity and enhancement data for each group of measurement techniques is shown in Figs. 6–26.

For each of the four measurement technique groupings, the average thermal conductivity is shown on the plot and is indicated by the solid line. In the custom THW data on Figs. 6 and 7, there is one measurement that is well above the average in both figures. This was the only THW apparatus with an uninsulated wire. Typically an insulated wire is used in this method to reduce the current leakage into the fluid. The higher thermal conductivity measured here may be a result of that effect. Excepting the outliers, all the measurement techniques show good agreement for de-ionized water (Figs. 7 and 16). For the PAO basefluid (Fig. 12) the uninsulated hot wire measurement (organization 14) is no longer an outlier. PAO is not as electrically conductive as water, and the current leakage effect should be less of an issue for this fluid.

As described in Appendix A, a fixed effects model was used to determine whether differences in the data from different measurement techniques are statistically significant. Because of the low number of data points in the parallel plate and Other categories, only the KD2 and custom hot wire techniques were compared. For all the samples in sets 1, 2, and 3, the KD2 thermal conductivity average is lower than the custom THW average. The fixed effects model shows that this is a statistically significant difference for samples 1, 3, 4, 6, and 7, in set 1, and sample 2 in set 3. In set 4, the KD2 average is higher than the Custom THW, but this difference is statistically significant only for sample 2 (the water+stabilizer basefluid for the ferrofluid). It is not clear why the KD2 measurements are lower than the THW measurements for all fluids except those in set 4. Finally, in most cases, there is less scatter in the KD2 data for the PAO-based nanofluids than the water-based nanofluids. This may be due to the higher viscosity of the PAO, which counteracts thermal convection during the 30 s KD2 heating cycle.

It is difficult to make specific conclusions about thermal conductivity measurements using the parallel plate technique due to the low number of data points and the amount of scatter for some samples (see Figs. 13–15). Additional measurements would be needed to determine if there is a systematic difference between the parallel plate technique and other techniques.

Although the thermal conductivity data show some clear differences in measurement technique, these differences become less apparent once the data are normalized with the basefluid thermal conductivities (Figs. 19–26). A comparison of the KD2 and THW techniques was again performed using the fixed effects model. The only statistically significant difference between the two techniques was for set 1, sample 4 (Fig. 21), the 3% volume fraction alumina-PAO nanofluid.

This study shows that the choice of measurement technique can affect the measured value of thermal conductivity, but if the enhancement is the parameter of interest, the measurement technique is less important, at least for the KD2 and THW techniques. Therefore, to ensure accurate determinations of nanofluid thermal conductivity enhancement using these techniques, it is important to measure both the basefluid and nanofluid thermal conductivity using the same technique and at the same temperature.

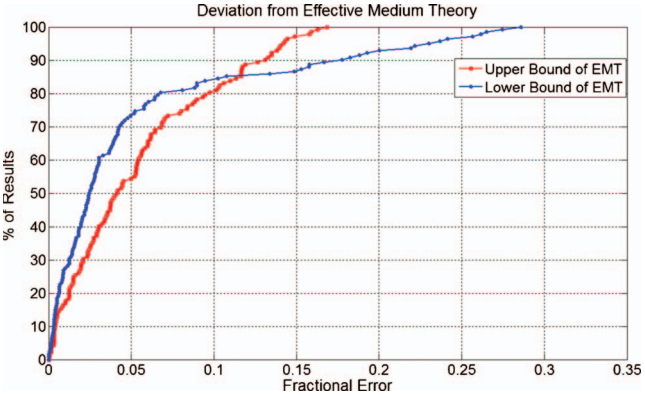

FIG. 27. (Color) Percentage of all INPBE experimental data that are predicted by the theory of Nan *et al.* within the error indicated on the *x*-axis.

V. COMPARISON OF DATA TO EFFECTIVE MEDIUM THEORY

Equation (1) is valid for well-dispersed noninteracting spherical particles with negligible thermal resistance at the particle/fluid interface. To include the effects of particle geometry and finite interfacial resistance, Nan *et al.*[51] generalized Maxwell's model to yield the following expression for the thermal conductivity ratio:

$$\frac{k}{k_f} = \frac{3 + \phi[2\beta_{11}(1 - L_{11}) + \beta_{33}(1 - L_{33})]}{3 - \phi(2\beta_{11}L_{11} + \beta_{33}L_{33})}, \tag{2}$$

where for particles shaped as prolate ellipsoids with principal axes $a_{11}=a_{22}<a_{33}$

$$L_{11} = \frac{p^2}{2(p^2-1)} - \frac{p}{2(p^2-1)^{3/2}}\cosh^{-1} p,$$

$$L_{33} = 1 - 2L_{11}, \quad p = a_{33}/a_{11},$$

$$\beta_{ii} = \frac{k_{ii}^c - k_f}{k_f + L_{ii}(k_{ii}^c - k_f)}, \quad k_{ii}^c = \frac{k_p}{1 + \gamma L_{ii} k_p/k_f},$$

$$\gamma = (2 + 1/p)R_{bd}k_f/(a_{11}/2),$$

and R_{bd} is the (Kapitza) interfacial thermal resistance. The limiting case of very long aspect ratio in the theory of Nan *et al.* is bounded by the nanoparticle linear aggregation models proposed by Prasher *et al.*[37], Keblinski *et al.*[52], and Eapen.[53] Obviously, Eq. (2) reduces to Eq. (1) for spherical particles ($p=1$) and negligible interfacial thermal resistance ($R_{bd}=0$), as it can be easily verified. Equation (2) predicts that, if $k_p > k_f$, the thermal conductivity enhancement increases with increasing particle loading, increasing particle aspect ratio and decreasing basefluid thermal conductivity, as observed for the data in INPBE set 1. More quantitatively, the theory was applied to the INPBE test nanofluids with the assumptions reported in Appendix B. Figure 27 shows the cumula-

tive accuracy information of the effective medium theory for all the INPBE data. Two curves are shown: one for zero interfacial thermal resistance (upper bound), and one for a typical value of the interfacial resistance, 10^{-8} m^2 K/W.[54–56] It can be seen that all INPBE data can be predicted by the lower bound theory with $<17\%$ error, while the upper bound estimate predicts 90% of the data with $<18\%$ error.

The above data analysis demonstrates that our colloidally stable nanofluids exhibit thermal conductivity in good agreement with the predictions of the effective medium theory for well-dispersed nanoparticles. That is, no anomalous thermal conductivity enhancement was observed for the nanofluids tested in this study. As such, resorting to the other theories proposed in the literature (e.g., Brownian motion, liquid layering, and aggregation) is not necessary for the interpretation of the INPBE database. It should be noted, however, that the ranges of parameters explored in INPBE, while broad, are not exhaustive. For example, only one nanofluid with metallic nanoparticles was tested, and only at very low concentration. Also, the temperature effect on thermal conductivity was not investigated.

VI. CONCLUSIONS

An international nanofluid property benchmark exercise, or INPBE, was conducted by 34 organizations participating from around the world. The objective was to compare thermal conductivity data obtained by different experimental approaches for identical samples of various nanofluids. The main findings of the study were as follows.

(1) The thermal conductivity enhancement afforded by the tested nanofluids increased with increasing particle loading, particle aspect ratio and decreasing basefluid thermal conductivity.
(2) For all water-based samples tested, the data from most organizations deviated from the sample average by $\pm 5\%$ or less. For all PAO-based samples tested, the data from most organizations deviated from the sample average by $\pm 10\%$ or less.
(3) The classic effective medium theory for well-dispersed particles accurately reproduced the INPBE experimental data; thus, suggesting that no anomalous enhancement of thermal conductivity was observed in the limited set of nanofluids tested in this exercise.
(4) Some systematic differences in thermal conductivity measurements were seen for different measurement techniques. However, as long as the same measurement technique at the same temperature conditions was used to measure the thermal conductivity of the basefluid, the thermal conductivity enhancement was consistent between measurement techniques.

ACKNOWLEDGMENTS

This work was made possible by the support of the National Science Foundation under Grant No. CBET-0812804. The authors are also grateful to Sasol and W. R. Grace & Co. for donating some of the samples used in INPBE. Special thanks to Mr. Edmund Carlevale of MIT for creating and maintaining the INPBE website.

APPENDIX A: STATISTICAL TREATMENT OF DATA

For each fluid sample, the thermal conductivity raw data $(x_{i1}, x_{i2}, \ldots, x_{in_i})$ from the ith organization were processed to estimate the organization's mean $(\bar{x}_i)$ and standard deviation (s_i), respectively, as

$$\bar{x}_i = \frac{1}{n_i}\sum_{j=1}^{n_i} x_{ij} \quad \text{and} \quad s_i = \sqrt{\frac{1}{n_i - 1}\sum_{j=1}^{n_i}(x_{ij} - \bar{x}_i)^2}. \tag{A1}$$

The values of $\bar{x}_i$ and s_i for each organization are shown in Figs. 6–18 as data points and error bars, respectively. The normality of the x_{ij} data sets was checked using the Shapiro–Francia W' test[57] and was found to be satisfactory. Peirce's criterion[58] was used to identify outliers which were not included in the sample average and variance calculations described below, but are shown in Figs. 6–18 as filled data points.

The analysis of data among different organizations was carried out using the random effects model.[57] In the random effects model, an assumption is made that the conclusions from the analysis can be applied to a wider class of measurements of which the n_i populations (or organizations, in this case) are a representative subset. The model assumes that

$$x_{ij} = \mu + \alpha_i + e_{ij}, \tag{A2}$$

where μ is the estimator of the sample mean, α_i is the systematic error for each organization (which are treated as random errors among organizations), and e_{ij} is the random or unexplained error for each measurement. It is helpful to note that

$$\alpha_i = \bar{x}_i - \mu,$$

$$e_{ij} = x_{ij} - \bar{x}_i. \tag{A3}$$

It is assumed that α_i and e_{ij} are normally distributed with zero means and standard deviations of σ_a and σ_e, respectively. The normality of the e_{ij} data sets was checked using the Shapiro–Francia W' test and was found to be satisfactory. This analysis assumes that standard deviations within the organizations are equal $(\sigma_i = \sigma_e)$. This was checked by performing pair-wise F-tests on σ_i.

The standard random effects model uses a weighted average as the sample average (taking into account the number of data points reported by each organization),

$$\mu = \bar{x} = \frac{1}{N}\sum_{i=1}^{I} n_i \bar{x}_i. \tag{A4}$$

We believe that this definition overemphasizes the contributions from organizations that reported many data points. For the purposes of this study, a more appropriate estimator of the sample mean is an unweighted average of organization averages given in the following equation:

TABLE VII. Input for effective medium model calculations.

	ϕ (%)	a_{11} (nm)	p	k_p (W/m K)	k_f (W/m K)	R_{bd} (m^2 K/W) Upper bound/lower bound
Set 1/sample 1	1	10	8	35	0.610	$0/10^{-8}$
Set 1/sample 3	1	81	1	35	0.161	$0/10^{-8}$
Set 1/sample 4	3	105	1	35	0.161	$0/10^{-8}$
Set 1/sample 5	1	10	8	35	0.161	$0/10^{-8}$
Set 1/sample 6	3	10	8	35	0.161	$0/10^{-8}$
Set 2/sample 1	0.001	15	1	315	0.610	$0/10^{-8}$
Set 3/sample 1	32	22	1	1.38	0.610	$0/10^{-8}$
Set 4/sample 1	0.17	7	1	4.25	0.461[a]	$0/10^{-8}$

[a]Sample average for sample 2 in Set 4.

$$\bar{x} = \frac{1}{I}\sum_{i=1}^{I} \bar{x}_i. \tag{A5}$$

This way, each organization contributes equally to the ensemble average. This estimator has been analyzed in the literature[57] and its variance is given by

$$\sigma^2 = \mathrm{Var}(\bar{x}) = \frac{1}{I^2}\sum_{i=1}^{I}\left(\frac{\sigma_e^2}{n_i} + \sigma_a^2\right), \tag{A6}$$

where

$$\sigma_e^2 = \frac{1}{(N-I)}\sum_{i=1}^{I}(n_i - 1)s_i^2, \tag{A7}$$

$$N = \sum_{i=1}^{I} n_i, \tag{A8}$$

$$\sigma_a^2 = \frac{(\mathrm{MSA} - \sigma_e^2)}{n_o}, \tag{A9}$$

$$\mathrm{MSA} = \frac{1}{(I-1)}\left(\sum_{i=1}^{I} n_i \bar{x}_i^2 - N\bar{x}^2\right), \tag{A10}$$

$$n_o = \frac{1}{I-1}\left(N - \frac{\sum_{i=1}^{I} n_i^2}{N}\right). \tag{A11}$$

The standard error (σ) of the unweighted average is shown in Figs. 6–18 as dotted lines plotted above and below the sample average. The literature shows that the estimator (A5) is preferred over the estimator (A4) if $\sigma_a^2 > \sigma_e^2$.[57,59] The statistical analysis shows that this condition is satisfied for the INPBE data.

Thermal conductivity enhancements were determined from the ratio of the nanofluid thermal conductivity to the basefluid thermal conductivity and are given as y_i. If an organizational mean for a given fluid sample was identified as an outlier in the thermal conductivity analysis, it was not excluded here in determining enhancements. A second round of applying the Peirce criterion excluded those enhancements that were outliers.

The standard deviation (error bars) of the thermal conductivity enhancements (data points) for individual organizations shown in Figs. 19–26 were calculated by propagating the standard deviation of the numerator and denominator.[60] That is, if $y = x_{\mathrm{nf}}/x_{\mathrm{bf}}$, then:

$$\frac{s_{\mathrm{enh}}}{y} = \sqrt{\left(\frac{s_{\mathrm{nf}}}{x_{\mathrm{nf}}}\right) + \left(\frac{s_{\mathrm{bf}}}{x_{\mathrm{bf}}}\right)}. \tag{A12}$$

The procedure for calculating the thermal conductivity enhancement sample average and its variance was based on Eqs. (A5)–(A11), where the thermal conductivity for each organization, $\bar{x}_i$, is replaced by the thermal conductivity enhancement for each organization, $\bar{y}_i$, and n_i is the harmonic average of the total number of measurements used to calculate the enhancement.

To compare the different measurement techniques, the fixed effects model was used.[57] For each technique, the technique average and the variance were determined using Eqs. (A5)–(A11) above. For an unbalanced data set (one in which there are a different number of data points for each measurement technique to be compared), the approximate Tukey–Kramer intervals were used, which depend on the probability statement,

$$P\left\{\mu_i - \mu_{i'} \in \bar{y}_i - \bar{y}_{i'} \pm q_{\alpha,k,\nu} s_i \left[\frac{1}{2}\left(\frac{1}{n_i} + \frac{1}{n_{i'}}\right)\right]^{1/2} \quad \text{for all } i,i'\right\} = 1 - \alpha, \tag{A13}$$

where $q_{\alpha,k,\nu}$ is the upper α point of the "studentized" range distribution for k (the number of measurement techniques compared) and ν, the degrees of freedom ($N-k$). If the interval given in Eq. (A12) does not contain zero for any combination of two measurement techniques, then the difference in technique mean is statistically significant.

APPENDIX B: ASSUMPTIONS USED IN THE EFFECTIVE MEDIUM MODEL FOR THERMAL CONDUCTIVITY

Use of the model of Nan *et al.* requires input of the values of the particle volumetric fraction (ϕ), particle minimum axis (a_{11}), particle aspect ratio (p), particle thermal conductivity (k_p), basefluid thermal conductivity (k_f), and

interfacial thermal resistance (R_{bd}). The nominal values used to generate the curves in Fig. 27 are shown in Table VII.

[1] J. A. Eastman, S. R. Phillpot, S. U. S. Choi, and P. Keblinski, Annu. Rev. Mater. Res. **34**, 219 (2004).
[2] S. K. Das, S. U. S. Choi, and H. E. Patel, Heat Transfer Eng. **27**, 3 (2006).
[3] S. Kabelac and J. F. Kuhnke, Annals of the Assembly for International Heat Transfer Conference, 2006 (unpublished), Vol. 13, p. KN-11.
[4] V. Trisaksri and S. Wongwises, Renewable Sustainable Energy Rev. **11**, 512 (2007).
[5] X. Q. Wang and A. S. Mujumdar, Int. J. Therm. Sci. **46**, 1 (2007).
[6] S. M. S. Murshed, K. C. Leong, and C. Yang, Appl. Therm. Eng. **28**, 2109 (2008).
[7] W. Yu, D. M. France, J. L. Routbort, and S. U. S. Choi, Heat Transfer Eng. **29**, 432 (2008).
[8] S. K. Das, S. U. S. Choi, W. Yu, and T. Pradeep, *Nanofluids: Science and Technology* (Wiley, New York, 2008).
[9] J. C. Maxwell, *A Treatise on Electricity and Magnetism*, 2nd ed. (Clarendon, Oxford, 1881).
[10] Q. Li and Y. M. Xuan, in *Heat Transfer Science and Technology*, edited by B. Wang (Higher Education Press, Beijing, 2000), pp. 757–762.
[11] J. A. Eastman, S. U. S. Choi, S. Li, W. Yu, and L. J. Thompson, Appl. Phys. Lett. **78**, 718 (2001).
[12] H. U. Kang, S. H. Kim, and J. M. Oh, Exp. Heat Transfer **19**, 181 (2006).
[13] T.-K. Hong, H. Yang, and C. J. Choi, J. Appl. Phys. **97**, 064311 (2005).
[14] S. Jana, A. Salehi-Khojin, and W. H. Zhong, Thermochim. Acta **462**, 45 (2007).
[15] M. Chopkar, P. K. Das, and I. Manna, Scr. Mater. **55**, 549 (2006).
[16] S. Shaikh, K. Lafdi, and R. Ponnappan, J. Appl. Phys. **101**, 064302 (2007).
[17] H. Xie, J. Wang, T. Xi, and F. Ai, J. Appl. Phys. **91**, 4568 (2002).
[18] H. Xie, J. Wang, T. Xi, and Y. Liu, Int. J. Thermophys. **23**, 571 (2002).
[19] S. M. S. Murshed, K. C. Leong, and C. Yang, Int. J. Therm. Sci. **44**, 367 (2005).
[20] C. H. Chon, K. D. Kihm, S. P. Lee, and S. U. S. Choi, Appl. Phys. Lett. **87**, 153107 (2005).
[21] K. S. Hong, T.-K. Hong, and H.-S. Yang, Appl. Phys. Lett. **88**, 031901 (2006).
[22] S. H. Kim, S. R. Choi, and D. Kim, ASME J. Heat Transfer **129**, 298 (2007).
[23] C. H. Li and G. P. Peterson, J. Appl. Phys. **101**, 044312 (2007).
[24] G. Chen, W. H. Yu, D. Singh, D. Cookson, and J. Routbort, J. Nanopart. Res. **10**, 1109 (2008).
[25] P. D. Shima, J. Philip, and B. Raj, Appl. Phys. Lett. **94**, 223101 (2009).
[26] S. K. Das, N. Putra, P. Thiesen, and W. Roetzel, ASME J. Heat Transfer **125**, 567 (2003).
[27] D. Wen and Y. Ding, J. Thermophys. Heat Transfer **18**, 481 (2004).
[28] C. H. Li and G. P. Peterson, J. Appl. Phys. **99**, 084314 (2006).
[29] H. D. Kumar, H. E. Patel, K. V. R. Rajeev, T. Sundararajan, T. Pradeep, and S. K. Das, Phys. Rev. Lett. **93**, 144301 (2004).
[30] S. P. Jang and S. U. S. Choi, Appl. Phys. Lett. **84**, 4316 (2004).
[31] R. Prasher, P. Bhattacharya, and P. E. Phelan, Phys. Rev. Lett. **94**, 025901 (2005).
[32] H. E. Patel, T. Sundararajan, T. Pradeep, A. Dasgupta, N. Dasgupta, and S. K. Das, Pramana, J. Phys. **65**, 863 (2005).
[33] H. E. Patel, T. Sundararajan, and S. K. Das, J. Nanopart. Res. **10**, 87 (2008).
[34] P. Keblinski, S. R. Phillpot, S. U. S. Choi, and J. A. Eastman, Int. J. Heat Mass Transfer **45**, 855 (2002).
[35] B. X. Wang, L. P. Zhou, and X. F. Peng, Int. J. Heat Mass Transfer **46**, 2665 (2003).
[36] M. Foygel, R. D. Morris, D. Anez, S. French, and V. L. Sobolev, Phys. Rev. B **71**, 104201 (2005).
[37] R. Prasher, W. Evans, P. Meakin, J. Fish, P. Phelan, and P. Keblinski, Appl. Phys. Lett. **89**, 143119 (2006).
[38] J. Eapen, J. Li, and S. Yip, Phys. Rev. E **76**, 062501 (2007).
[39] J. Philip, P. D. Shima and R. Baldev, Nanotechnology **19**, 305706 (2008).
[40] W. Yu and S. U. S. Choi, J. Nanopart. Res. **5**, 167 (2003).
[41] J. Eapen, J. Li, and S. Yip, Phys. Rev. Lett. **98**, 028302 (2007).
[42] J. Eapen, W. C. Williams, J. Buongiorno, L. W. Hu, S. Yip, R. Rusconi, and R. Piazza, Phys. Rev. Lett. **99**, 095901 (2007).
[43] R. K. Iler, *The Chemistry of Silica* (Wiley, New York, 1979), Chap. 4.
[44] J. G. Gutierrez and M. Riccetti, Proceedings of the ASME International Mechanical Engineering Congress and Exposition, Boston, Massachusetts, 31 October–6 November 2008 (unpublished).
[45] J. J. Healy, J. J. de Groot, and J. Kestin, Physica C **82**, 392 (1976).
[46] T. Boumaza and J. Redgrove, Int. J. Thermophys. **24**, 501 (2003).
[47] R. G. Miller and L. S. Fletcher, Proceedings of the Tenth Southeastern Seminar on Thermal Sciences, New Orleans, LA, 1974 (unpublished), pp. 263–285.
[48] H. Ziebland, in *Thermal Conductivity*, edited by R. P. Tye (Academic, London, 1969), Vol. 2, pp. 96–110.
[49] R. W. Powell, in *Thermal Conductivity*, edited by R. P. Tye (Academic, London, 1969), Vol. 2, pp. 288–295.
[50] H. Eichler, G. Salje, and H. Stahl, J. Appl. Phys. **44**, 5383 (1973).
[51] C. W. Nan, R. Birringer, D. R. Clarke, and H. Gleiter, J. Appl. Phys. **81**, 6692 (1997).
[52] P. Keblinski, R. Prasher, and J. Eapen, J. Nanopart. Res. **10**, 1089 (2008).
[53] J. Eapen, *Thermal conduction mechanism in nanofluids, solid composites and liquid mixtures*, Proceedings of 2009 ASME Summer Heat Transfer Conference (HT2009-88236), July 19-23, 2009, San Francisco, CA.
[54] O. M. Wilson, X. Hu, D. G. Cahill, and P. V. Braun, Phys. Rev. B **66**, 224301 (2002).
[55] S. Huxtable, D. G. Cahill, S. Shenogin, L. Xue, R. Ozisik, P. Barone, M. Usrey, M. S. Strano, G. Siddons, M. Shim, and P. Keblinski, Nature Mater. **2**, 731 (2003).
[56] E. V. Timofeeva, A. N. Gavrilov, J. M. McCloskey, Y. V. Tolmachev, S. Sprunt, L. M. Lopatina, and J. V. Selinger, Phys. Rev. E **76**, 061203 (2007).
[57] R. G. Miller, *Beyond ANOVA, Basics of Applied Statistics* (CRC, Boca Raton, 1997), pp. 69–111.
[58] S. M. Ross, J. Engineering Technology **20**, 38 (2003).
[59] G. W. Snedecore and W. G. Cochran, *Statistical Methods* (Iowa State University Press, Ames, 1989).
[60] H. Motulsky, *Intuitive Biostatistics* (Oxford University Press, New York, 1995), pp. 284–286.
[61] J. Glory, M. Bonetti, M. Helezen, M. Mayne-L'Hermite, and C. Reynaud, J. Appl. Phys. **103**, 094309 (2008).
[62] N. Shalkevich, W. Escher, T. Buergi, B. Michel, L. Si-Ahmed, and D. Poulikakos, "On the thermal conductivity of gold nanoparticle colloids," Langmuir (in press).
[63] D. C. Venerus, M. S. Kabahdi, S. Lee, and V. Perez-Luna, J. Appl. Phys. **100**, 094310 (2006).
[64] J.-H. Lee, K. S. Hwang, S. P. Jang, B. H. Lee, J. H. Kim, S. U. S. Choi, and C. J. Choi, Int. J. Heat Mass Transfer **51**, 2651 (2008).
[65] R. Rusconi, W. C. Williams, J. Buongiorno, R. Piazza, and L. W. Hu, Int. J. Thermophys. **28**, 1131 (2007).
[66] J. Garg, B. Poudel, M. Chiesa, J. B. Gordon, J. J. Ma, J. B. Wang, Z. F. Ren, Y. T. Kang, H. Ohtani, J. Nanda, G. H. McKinley, and G. Chen, J. Appl. Phys. **103**, 074301 (2008).
[67] J. Townsend and R. Christianson, Proceedings of the 17th Symposium on Thermophysical Properties, Boulder, CO, 21–16 June 2009 (unpublished).
[68] A. Jarzebski, M. Palica, A. Gierczycki, K. Chmiel-Kurowska, and G. Dzido, Silesian University of Technology Internal Report No. BW-459/RCh6/2007/6, 2007.
[69] B. Wright, D. Thomas, H. Hong, L. Groven, J. Puszynski, D. Edward, X. Ye, and S. Jin, Appl. Phys. Lett. **91**, 173116 (2007).
[70] P. E. Gharagozloo and K. E. Goodson, Appl. Phys. Lett. **93**, 103110 (2008).
[71] S. Van Vaerenbergh, T. Maré, C. Tam Nguyen, and A. Guerin, VIII-ème Colloque Interuniversitaire Franco-Québécois sur la Thermique des Systèmes, Montréal, Canada, 28–30 May 2007 (unpublished).
[72] D. Wen and Y. Ding, IEEE Trans. Nanotechnol. **5**, 220 (2006).
[73] J. G. Gutierrez and R. Rodriguez, Proceedings of the ASME International Mechanical Engineering Congress and Exposition, Seattle, Washington, 11–15 November 2007 (unpublished).